Available online at www.sciencedirect.com
ScienceDirect
Applied Catalysis B: Environmental 79 (2008) 382–393
APPLIED CATALYSIS B: ENVIRONMENTAL
www.elsevier.com/locate/apcatb

Temperature programmed desorption/surface-reaction study of an anodic alumina supported Ag catalyst for selective catalytic reduction of nitric oxide with propene

Yu Guo *, Makoto Sakurai, Hideo Kameyama

Department of Chemical Engineering, Tokyo University of Agriculture and Technology, 24-16 Nakacho 2, Koganei-shi, Tokyo 184-8588, Japan

Received 4 March 2006; received in revised form 27 October 2007; accepted 3 November 2007
Available online 12 November 2007

Abstract

On an anodic alumina supported silver catalyst with a low Ag loading (1.68 wt.%), NO_x (NO/He, NO/O_2/He, NO_2/He) adsorption measurements and NO_x-temperature programmed decomposition (TPD)/temperature programmed surface-reaction (TPSR) measurements in different gas streams (He, C_3H_6/He, C_3H_6/O_2/He) were conducted to investigate the formation, consumption and reactivity of surface adsorbed NO_x species.

During NO adsorption, no noticeable uptake of NO was detected. Introducing oxygen greatly improved the formation of ads-NO_x species. A greater quantity of surface nitrate species was found after NO_2 adsorption, accompanied with gaseous NO release. The result of TPSR demonstrates the surface nitrate species can be effectively and preferentially reduced by propene. When introducing oxygen into the propene gas stream of TPSR test, the significantly increased amount of reacted nitrate undoubtedly shows the importance of oxygen in activating propene. The pathway for the selective reduction of NO_x in the presence of excess oxygen is proposed to pass through the selective reduction of the adsorbed nitrate species with the activated propene.

The enhanced NO_x conversion when replacing NO with NO_2 was attributed to the stronger NO_x adsorption capacity and oxidation ability of NO_2, than those for NO. With increasing oxygen concentration, the difference between NO and NO_2 would gradually decrease, and finally disappear in a high excess of oxygen.

Keywords: Ag; Anodic alumina; TPD/TPSR; Selective catalytic reduction; De-NO

1. Introduction

Selective catalytic reduction of nitric oxide with hydrocarbons (HC-SCR of NO) has received much attention as a possible means of controlling emissions from diesel engines operating under oxygen-rich conditions. In the last decade, Ag/alumina catalyst was considered one of the most promising de-NO_x catalysts, and was extensively investigated using methane [1], propene [2–5,6], propane [6,7], long paraffins [8,9] and alcohols [10–12] as reductants, due to its relatively high and durable de-NO_x activity even in the presence of SO_x and water, moderate operating temperature window (573–723 K) and inexpensive preparation cost.

In Ag/alumina, Ag loading is the most crucial parameter affecting the de-NO_x activity. When using low or moderate Ag loadings (1–3 wt.%), silver oxide species and increased dispersion were observed, and higher conversions were also attained [13–18]. On the contrary, increasing silver loading was related to the formation of metallic Ag on the catalytic surface, which favored oxidation of the reductant by oxygen, and led to limited de-NO_x activity [19]. Besides, catalysts with higher Ag loadings were also found to produce significant amounts of N_2O [15,16]. In a recent review on HC-SCR of NO_x, it was suggested that different Ag loadings resulted in different catalytic phases, which were related to different reaction pathways [16]. Bogdanchikova et al. [20] revealed that the oxidation of NO with O_2 into NO_2 was catalyzed by crystalline metallic silver, whereas HC-SCR of NO_x was promoted by

* Corresponding author at: Kameyama & Sakurai Laboratory, Department of Chemical Engineering, Tokyo University of Agriculture and Technology, 24-16 Nakacho 2, Koganei-shi, Tokyo 184-8588, Japan. Tel.: +81 42 388 7066; fax: +81 42 388 7248.
E-mail address: mguoyu@cc.tuat.ac.jp (Y. Guo).

0926-3373/$ – see front matter © 2007 Elsevier B.V. All rights reserved.
doi:10.1016/j.apcatb.2007.11.002

Ag(I). The fact that Ag/alumina with low or moderate Ag loading is effective for NO_x reduction, but is inactive in NO oxidation into NO_2 with O_2 [20] suggests that in Ag/alumina the oxidation of NO is not a crucial reaction step in HC-SCR of NO_x as it is on other catalysts. Several authors focussed on a reaction mechanism in which hydrocarbon reducing agent was activated through partial oxidation. This activated hydrocarbon was proposed to react with nitrates on the catalyst surface to form organic nitrate intermediates, and finally lead to nitrogen and carbon oxides [8,21–23]. Some reaction steps of the HC-SCR of NO_x reaction occurred in homogeneous gas-phase. Oxygenated hydrocarbons adsorbed on the catalyst surface (acetate) were observed with in situ Fourier-Transform infrared (FTIR) spectroscopy in HC-SCR of NO_x using propene [24,25], hexane [8], octane [26] and so on. The reaction between partially oxygenated hydrocarbon and adsorbed NO_x species leads to the formation of isocyanate (−NCO) species observed with in situ diffuse reflectance infrared Fourier-Transform (DRIFT) spectroscopy and assumed to be key reaction intermediates [10]. The absence of appreciable activity of Ag/alumina at low temperatures was ascribed to the inhibition of active sites due to adsorbed nitrates [4,8,21,24].

Many reviews on the present reaction discuss the conventional process, which is carried out on bead catalysts in fixed bed reactors. However, this reactor suffers from several drawbacks, such as a poor heat transfer coefficient, diffusion limitations, great pressure drop and large volume size. Consequently, constructed wall type reactors have become the focus of recent research, due to their excellent gas diffusion and heat transmission and compact size. For the preparation of a plate catalyst, though various methods have been reported, such as sol–gel coating and nano-particle-based coating, the thermal endurance of the catalysts was seldom mentioned. At high temperatures, it is difficult to prevent the coating layers peeling from the base materials due to the difference in their thermal expansions. To avoid such a problem, a novel metal-monolithic plate-type anodic alumina catalyst with high thermal endurance and conductivity was developed by Kameyama et al. [27,28]. Porous alumina film can be formed on the surface of Al plate by anodization. Hot water treatment and subsequent calcination greatly increase the film's surface area, making it comparable to even some types of commercial bead alumina [29]. Since the alumina layer is derived from the base material, a close uniformity throughout the alumina layers can effectively prevent the mismatch in thermal expansion. The thermal endurance test showed a high heat resistance, and the alumina layer was not observed to peel from the catalyst during a test of up to 40,000 heating cycles [30]. Furthermore, since anodization is conducted in aqueous solution, a base material with a complex structure such as mesh, serrated honeycomb or spiral shape, can easily be prepared into an alumina support that allows a low-pressure drop.

In this paper, we prepared an anodic alumina supported Ag catalyst with a low loading (1.68 wt.%) to investigate the formation, consumption and reactivity of surface nitrate species through NO_x adsorption, and NO_x-temperature programmed decomposition (TPD) and -temperature programmed surface-reaction (TPSR) measurements, to gain new insights into the practicability of this catalyst and the mechanism in HC-SCR. Here, we focused on the mechanism of HC-SCR over this catalyst; a comparison investigation between the anodic alumina catalyst and the conventional alumina catalyst will be discussed elsewhere later.

2. Experimental

2.1. Catalyst preparation and characterization

Details regarding the preparation of the plate-type anodic γ-alumina support (Al_2O_3 (100 μm)/Al (100 μm)/Al_2O_3 (100 μm)) have been given elsewhere [29]. Using the plate-type anodic alumina support (131.3 $m^2\ g^{-1}$), an anodic alumina supported Ag catalyst with Ag loading of 1.68 wt.% and specific surface area of 128.6 $m^2\ g^{-1}$, designated $Ag/Al_2O_3/Al$, was prepared with the solution impregnation method. The support was impregnated using an aqueous solution containing a sufficient amount of $AgNO_3$ for 1 h under ambient conditions. The plate was then dried naturally for 4 h, and calcined in air at 773 K for 3 h.

The thickness of the resulting alumina film was measured by the eddy current probe method (T3.3B, ANOTECH). BET specific surface area and pore radius were measured by a nitrogen adsorption method (SA3100, Beckman Coulter, Inc.). Ag loading was analyzed by atomic absorption spectrometry (AA-680, Shimadzu Corp.), and is reported here based on the quantity of the surface alumina layer. Unless otherwise stated, the quantity of the inner Al layer was excluded from the calculation of the quantity of the plate-type catalyst.

2.2. De-NO_x catalytic reactions

A fixed bed quartz reactor (i.d. 6 mm) was used to test the de-NO_x activity of the synthesized $Ag/Al_2O_3/Al$ catalyst. The plate-type catalyst was cut into small pieces (ca. 5 mm^2) and packed in the reactor, using quartz sand for dilution with a loading density of 0.4 $cm^2_{catalyst}\ (g_{quartzsand})^{-1}$. Both inlet and outlet stream mixtures were analyzed with gas chromatographs: C_3H_6 (FID), O_2, N_2, N_2O and CO_2 (TCD). NO_x (NO and NO_2) was measured with a PG-250 portable gas analyzer with NO_x, NO, CO and O_2 detectors (Horiba, Ltd.). The reactor temperature was controlled with a programmable temperature controller (818P4, Eurotherm Inc.). The reaction feed stream was prepared by mixing certified and analyzed model gases (supplied by Tohei Industrial Co. Ltd.), with helium as the base gas. The total gas flow rate was set at 150 mL min^{-1} (i.e., F/W = 65,000 mL $g^{-1}\ h^{-1}$).

The results obtained were evaluated in terms of NO_x conversion, N_2O yield, NO_2 yield and C_3H_6 conversion. NO_x conversion was defined as $((NO + NO_2)_{inlet} - (NO + NO_2)_{outlet})/(NO + NO_2)_{inlet} \times 100\%$. N_2O yield and NO_2 yield were expressed as follows: $N_2O\ \text{yield} = 2 \times N_2O_{produced}/(NO + NO_2)_{inlet} \times 100\%$; $NO_2\ \text{yield} = NO_{2\ \text{produced or remaining}}/(NO + NO_2)_{inlet} \times 100\%$. The C_3H_6 conversion was calculated as $(C_3H_{6\ inlet} - C_3H_{6\ outlet})/C_3H_{6\ inlet} \times 100\%$.

2.3. Adsorption, TPD and TPSR studies

Adsorption, TPD and TPSR tests were carried out using the same catalytic reaction apparatus. The same fixed bed quartz reactor was used to load the catalyst, and the sample quantity and loading method were the same as in the aforementioned activity test. The sample was pretreated at 673 K in He for 1 h to remove adsorbed H_2O and other gases, and then cooled to 298 K. The pretreated sample was exposed to the appropriate gas mixture with a flow of 150 mL min^{-1} (1000 ppm NO/He, 1000 ppm NO/15% O_2/He, 1000 ppm NO_2/He, 1000 ppm NO_2/15% O_2/He) at 298 K until saturated adsorption, and the adsorption of inlet compositions was recorded online as a function of adsorption time using the portable gas analyzer. Subsequently, the sample was purged with 150 mL min^{-1} of He at 298 K until the concentration of adsorption gas in He returned to zero level, which was monitored by the portable gas analyzer. A TPD or TPSR run was started from 298 to 823 K at a ramping rate of 10 K min^{-1} in different gas mixtures with a flow of 150 mL min^{-1} (He, 5000 ppm C_3H_6/He, 5000 ppm C_3H_6/15% O_2/He). In addition, for each adsorption in the TPD and TPSR tests, a corresponding blank test was also conducted under the same conditions to correct for the measurement background.

A mass spectrometer (AERO VAC, Vacuum Technology Inc.) was used to continuously monitor the effluent from the reactor, which contained N_2/CO ($m/z = 28$), NO ($m/z = 30$), O_2 ($m/z = 32$), C_3H_6 ($m/z = 41$, main mass of propene corresponding to $C_3H_5^+$ [31]), N_2O/CO_2 ($m/z = 44$) and NO_2 ($m/z = 46$). It should be noted that the NO_2 signal at $m/z = 46$ was not detected with our mass spectrometer. Even when 1000 ppm NO_2/He was used, the intensity corresponding to a mass number of 46 was still too weak to be detected (but the $m/z = 30$ signal was strong). Additionally, in TPSR, the formation profile for a mass number of 44 was confirmed to be from both the decomposition product (N_2O, $m/z = 44$) of NO_x and the oxidation product (CO_2, $m/z = 44$) of C_3H_6. Similarly, the formation profile for a mass number of 28 was from the reduction product (N_2, $m/z = 28$) of NO_x and the oxidation product (CO, $m/z = 28$) of C_3H_6. Therefore, two different analyzers, the portable gas analyzer and the mass spectrometer, were combined for our outflow-online detection system. The portable gas analyzer was used to analyze NO_x, NO, NO_2 ($[NO_2] = [NO_x] - [NO]$), O_2 (only in the adsorption test) and CO. The mass spectrometer monitored the signal of N_2/CO, O_2, C_3H_6 and N_2O/CO_2.

3. Results and discussion

3.1. De-NO_x catalytic reactions

The de-NO_x reactivity of the synthesized $Ag/Al_2O_3/Al$ catalyst was tested under different SCR conditions, and the activity difference between NO and NO_2 is also discussed. The results are shown in Fig. 1((a) NO_x conversion, (b) C_3H_6 conversion, (c) N_2O yield, (d) NO_2 yield (in the case of using NO) and (e) NO_2 yield (in the case of using NO_2)).

Without C_3H_6 (i.e., 1000 ppm NO or NO_2/15% O_2/He), a measurable NO_x conversion was detected for neither NO nor NO_2. Introducing C_3H_6 substantially improved NO_x reduction, and the plot of NO_x conversion was shifted to a lower temperature region with increasing C_3H_6 concentration. In the case of 1000 ppm NO or NO_2/5000 ppm C_3H_6/15% O_2/He (or 5000 ppm NO or NO_2/5000 ppm C_3H_6/15% O_2/He), the comparison C_3H_6 conversion with NO_x conversion shows that C_3H_6 oxidation is coincident with NO_x reduction. That is, NO_x reduction improved as propene was effectively oxidized, however, once C_3H_6 conversion approached 100%, NO_x reduction was depressed. Thus, the lack of propene available for NO_x reduction is responsible for the loss of NO_x conversion at high temperatures. Additionally, the temperature where NO_x reduction initiated was observed to closely depend on the ''light-off'' temperature for C_3H_6 oxidation (ca. 573 K). These results clearly reveal a critical role of C_3H_6 in the HC-SCR of NO_x. Similar to the propene behavior, increasing oxygen concentration with a constant propene concentration significantly promoted NO_x reduction, and shifted the plot of NO_x conversion to lower temperatures.

In Fig. 1a, under all 15% oxygen conditions, an activity difference between NO and NO_2 was not found, though the propene concentration increased from 0 to 5000 ppm. In contrast, the difference became very significant when decreasing the oxygen concentration to 2% or zero. For example, in the case of 1000 ppm NO/5000 ppm C_3H_6/He, there was no noticeable NO_x conversion until the temperature exceeded 773 K, while NO_x conversion increased to 22% at 673 K when NO was replaced by NO_2. Meanwhile, in the case of 1000 ppm NO or NO_2/1000 ppm C_3H_6/2% O_2/He, the variation in propene conversion along with switching from NO to NO_2 revealed that propene oxidation was remarkably improved. However, the small increase in the ratio of increased oxygen atoms from NO_2 to total oxygen atoms (4.8%) seemingly conflicts with the substantial increase in propene conversion, which may require new explanation. A detailed discussion will be carried out later.

N_2O yield, a primary by-product of NO_x reduction, was measured and is presented in Fig. 1c. N_2O yield under all conditions was very low, even negligible if compared with the high NO_x conversion. Nevertheless, the N_2O yield was found to slightly increase with increasing oxygen concentration, and a small but measurable increment was also detected when using NO_2 instead of NO. Generally, the promotional effects of oxygen and NO_2 and the small amount of N_2O formation are considered the main characteristics of selective catalytic reduction of NO_x with hydrocarbons, rather than NO_x direct decomposition [32].

Fig. 1d shows the NO_2 yield (NO_2 produced) obtained in the cases using NO, and the dotted line represents the thermodynamic limit of NO_2 yield associated with the equilibrium reaction: $2NO + O_2 \leftrightarrow 2NO_2$. The NO_2 yield of 3% in the blank test (without catalyst and reductant) is related to the oxidation reaction of NO into NO_2 occurring in the dead volume of the reaction apparatus. In a comparison of NO_2 yields in 1000 ppm NO/15% O_2/He and the blank test, the $Ag/Al_2O_3/Al$ catalyst did

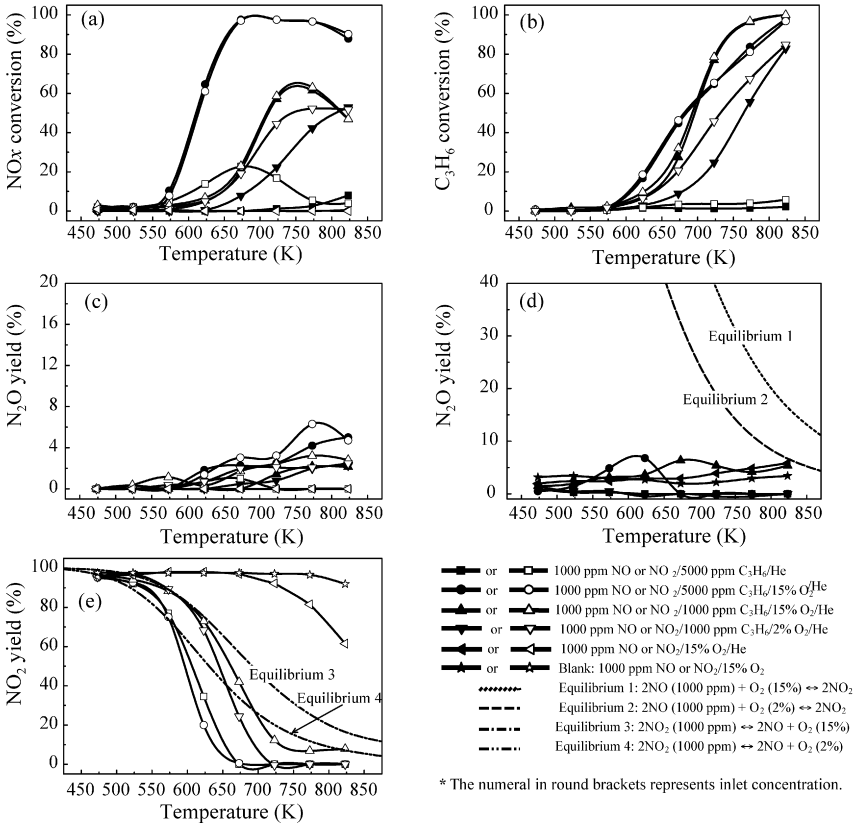

Fig. 1. Catalytic activity of $Ag/Al_2O_3/Al$ under different conditions as a function of temperature. (a) NO_x conversion, (b) C_3H_6 conversion, (c) N_2O yield, (d) NO_2 yield in the case using NO, (e) NO_2 yield in the case using NO_2.

not exhibit any remarkable ability to oxidize NO into NO_2, and the NO_2 yield was far from the thermodynamic limit, at least until 823 K. The fact that $Ag/Al_2O_3/Al$ is effective in NO_x reduction but inactive for NO oxidation, suggests that NO oxidation into NO_2 may not be a crucial reaction step in HC-SCR of NO on $Ag/Al_2O_3/Al$, as it is on other catalysts. In addition, in the presence of propene, the NO_2 yield showed a slight increase from the initial temperature of NO_x reduction, but quickly decreased before the NO_x reduction peak appeared.

The NO_2 yield (remaining NO_2) in the NO_2 case is presented in Fig. 1e. In the absence of reductant, due to the poor thermal stability of NO_2: $2NO_2 \leftrightarrow 2NO + O_2$, remarkable decomposition of NO_2 was detected on the $Ag/Al_2O_3/Al$ catalyst, but far from the thermodynamic limit. However, under all conditions in which propene was present, the NO_2 yield sharply decreased and exceeded the thermodynamic limit from the ''light-off'' temperature for propene oxidation (ca. 573 K). It is clear that the decrease in NO_2 yield does not coincide with the order of the corresponding NO_x conversion, but was greatly influenced by the amount of propene. These results suggest that an incomplete reduction of NO_2 into NO with propene, rather than the poor thermal stability of NO_2, should be responsible for this decline in NO_2 yield. To further study this phenomenon, a reference blank test without catalyst was carried out in 1000 ppm NO_2/5000 ppm C_3H_6/15% O_2/He, as shown in Fig. 2. The decreased NO_2 yield clearly exceeded the thermodynamic limit of NO_2 decomposition at high temperatures, whereas NO_x reduction was very low and even negligible. Besides, the decrease in NO_2 yield greatly accelerated as propene conversion obviously appeared. These results indicate that the incomplete reduction of NO_2 into NO can even occur in homogeneous gas-phase, and the presence of catalyst aggravates this process as propene is effectively oxidized.

In Sections 3.2 and 3.3, NO_x adsorption measurements (NO/He, NO/O_2/He, NO_2/He, NO_2/O_2/He) under ambient conditions without reductant, and NO_x-TPD and -TPSR measurements in different gas streams (He, C_3H_6/He, C_3H_6/O_2/He) were investigated for further interpretation of phenomena in steady-state experiments.

3.2. NO_x adsorption and TPD studies

3.2.1. NO adsorption

NO adsorption on the $Ag/Al_2O_3/Al$ catalyst at 298 K was recorded as a function of adsorption time, as shown in Fig. 3. The adsorption of NO gave an S-type profile, reflecting the adsorption and saturation of the catalyst with NO. Throughout the entire NO adsorption, no remarkable NO uptake was observed, and NO_2 formation was hardly detected. NO adsorption reached complete saturation just after 1 min of NO inlet, almost the same as a blank test without catalyst (not shown here). The result indicates little NO adsorbs on catalyst in the absence of oxygen.

The TPD test in flowing He after NO adsorption is shown in Fig. 4(a) ms-signal and (b) PG-250 gas analyzer. TPD profiles did not show a noticeable desorption peak for NO_x, except for a

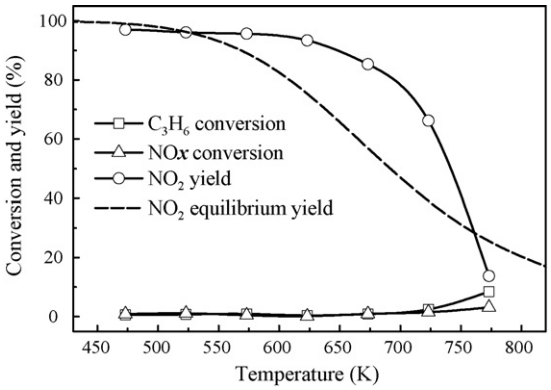

Fig. 2. Activity performance in a blank reactor without catalyst as a function of temperature. (NO_2: 1000 ppm, C_3H_6: 5000 ppm, O_2: 15%; the dotted line is associated with the equilibrium reaction: $2NO_2 \leftrightarrow 2NO + O_2$).

desorption peak for NO at 440 K with a low evolution amount that could be ascribed to the weakly adsorbed NO_x species. The formation of N_2O ($m/z = 44$) was recorded from ca. 450 K, and its signal became relatively intense from 700 K, though still very small. Similarly, a nitrogen formation signal with a very minute intensity was also observed from almost the same temperature. The oxygen signal was not detected during this TPD test.

3.2.2. NO/O_2 coadsorption

Fig. 5 shows the coadsorption of NO and O_2 on the Ag/Al_2O_3/Al catalyst. In the presence of oxygen, the adsorption of NO approached a saturated state after ca. 140 min of NO/O_2/He inlet, reflecting a very large NO adsorption capacity. In Table 1, the adsorption amount of NO_x in different gas streams (NO/He, NO/O_2/He, NO_2/He and NO_2/O_2/He) was calculated by integrating the adsorption curve and subtracting the background obtained from the corresponding blank test. Comparing the NO_x uptake in NO/O_2/He with that in ''NO only'' clearly shows the presence of oxygen greatly enhances the NO_x adsorption capacity from 19.7 to 315.2 μmol g^{-1}, even though the catalyst was pretreated with the same procedure. Uptake of NO was hardly observed when NO was introduced without oxygen, indicating in the NO and O_2 coadsorption NO adsorbed in the oxidized states, maybe nitrites and/or nitrates. In addition, during coadsorption, NO_2 evolution, which originated from the oxidation of NO with O_2, gradually rose at a slower speed than did NO evolution. That is, NO_2 appeared gradually as the adsorption of NO approached a saturated state. This result suggests some NO_2 probably directly participates in the adsorption process.

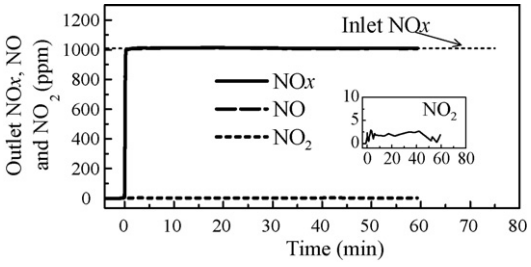

Fig. 3. Dependence of outlet concentrations of NO_x, NO and NO_2 on adsorption time of the Ag/Al_2O_3/Al catalyst in flowing 1000 ppm NO/He at 298 K.

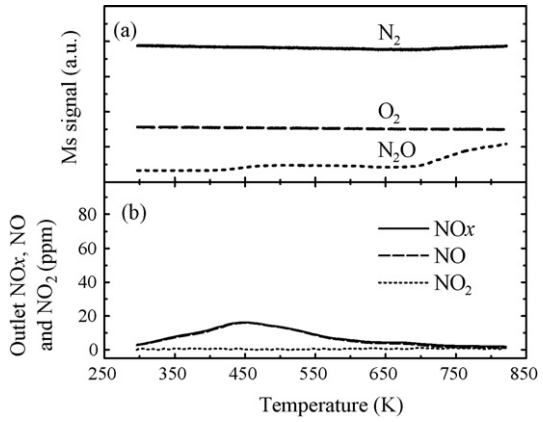

Fig. 4. TPD profiles (a) outlet ms-signals of N_2, O_2 and N_2O; (b) outlet concentrations of NO_x, NO and NO_2, in flowing He after exposure of the Ag/Al_2O_3/Al catalyst to 1000 ppm NO/He.

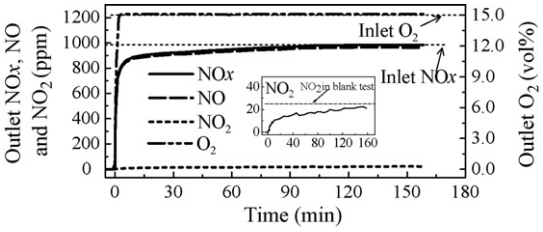

Fig. 5. Dependence of outlet NO_x, NO, NO_2 and O_2 concentrations on adsorption time of the Ag/Al_2O_3/Al catalyst in flowing 1000 ppm NO/15% O_2/He at 298 K.

Fig. 6 depicts the result of the TPD test in flowing He after coadsorption of NO and O_2. At first, the desorption curve of NO_x was integrated to volumetrically determine the desorption amount of NO_x, and the result is shown in Table 2. The amount of NO_x desorption, 322.9 μmol g^{-1}, clearly indicates that the adsorbed NO_x in the coadsorption of NO and O_2 is completely evacuated in the He gas stream before 823 K. Both NO and NO_2 desorption profiles displayed a low temperature (LT) desorption peak and a high temperature (HT) desorption peak. At low temperatures, the desorbed NO increased with increasing temperature from 298 K and had a maximum of 230 ppm at 359 K, and then dropped gradually. After the drop, a very weak HT peak was initiated from 500 K, and there was a maximum of 24.5 ppm at 760 K. In contrast, the NO_2 desorption had a

Table 1
Volumetric determination of NO_x adsorption on the Ag/Al_2O_3/Al catalyst at 298 K

Adsorption gas	Adsorption amount of NO_x[a] (μmol g^{-1})
1000 ppm NO/He	19.7
1000 ppm NO/15% O_2/He	315.2
1000 ppm NO_2/He	534.6
1000 ppm NO_2/15% O_2/He	527.1

[a] The integral value obtained in corresponding blank experiment has been subtracted.

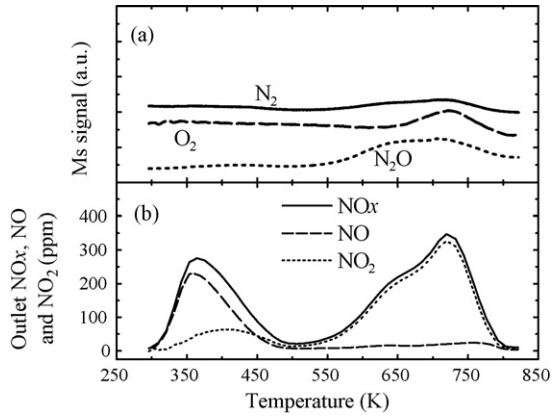

Fig. 6. TPD profiles (a) outlet ms-signals of N_2, O_2 and N_2O; (b) outlet concentrations of NO_x, NO and NO_2, in flowing He after exposure of the $Ag/Al_2O_3/Al$ catalyst to 1000 ppm NO/15% O_2/He.

weaker LT peak in the range of 298–500 K (maximum NO_2 of 64 ppm at 410 K) and a stronger HT peak at 550–823 K (maximum NO_2 of 327 ppm at 720 K). Concomitantly, the desorption peak for oxygen, as well as the formation peaks of N_2 and N_2O, were observed at the same temperature as the HT desorption peak for NO_2. In addition, it should be commented that not only the supported Ag but also the anodic alumina participated into the NO_x adsorption, because the amount of ads-NO_x in the coadsorption of NO and O_2 (315.2 μmol g^{-1}) is higher than the amount of supported Ag (155.6 μmol g^{-1}). In this study, the supported Ag and alumina support are considered as a whole, and an investigation into the adsorption performance of the anodic alumina will be discussed elsewhere later.

The adsorption and desorption of NO and NO/O_2 on alumina, silver polycrystalline foil and alumina-supported silver catalyst has been studied by several groups. Bao et al. [33] studied coadsorption of NO and O_2 on a Ag (1 1 0) surface using XPS, UPS, and Raman spectroscopy, and found that the existence of oxygen enhanced the adsorption of NO_x species. When they introduced a 1:10 mixture of NO/O_2 at 375 K, both NO_2^- and NO_3^- species were formed. Müslehiddinoğlu et al. [34] reported the result for NO adsorption/desorption on a Ag(13 wt.%)/α-Al_2O_3 catalyst with different pretreatments. They proposed that a nitrite species, rather than a nitrate species, was formed after exposure to "NO only" (i.e., either gaseous oxygen or surface covered oxygen was absent), whereas in the coadsorption of NO and O_2, an obvious nitrate species was detected by XRD analysis, even on a Ag/α-Al_2O_3 catalyst reduced by H_2. Zemlyanov et al. [35,36] investigated the reaction between Ag foil and a mixture of NO/O_2 at 300 K using XPS, ISS, and SEM to identify a complicated sandwich structure consisting of superimposed $AgNO_3$ and Ag_2O layers at the surface of metallic Ag. $AgNO_3$ formation was thought to proceed via the reaction between silver and NO_2 formed by the conversion of NO in an excess of oxygen [37]. In addition, some research into the NO_2 adsorption on silver catalyst [34,38–40] indicated that the formation of NO_3^- species occurred regardless of the temperature range or the form of Ag. This literature overview implies that the role of oxygen in the formation process of nitrate species after the exposure of silver catalyst to NO/O_2 is its promotional effect on the formation of NO_2 via the temperature dependent equilibrium, i.e., $2NO + O_2 \leftrightarrow 2NO_2$.

3.2.3. NO_2 adsorption

To investigate the adsorption behavior of NO_2 on the $Ag/Al_2O_3/Al$ catalyst, a similar adsorption experiment was carried out in flowing 1000 ppm NO_2/He. The result is shown in Fig. 7. First, there was a complete NO_x uptake for a short time revealed by an initial zero concentration of outlet NO_x concentration. The outlet NO concentration then sharply increased from a time defined as the starting time, reached a plateau at 5 min, maintaining 335 ± 11 ppm for 6 min, while NO_2 remained absent in the outlet stream. The outlet NO and NO_2 then resumed their inlet values, and saturation was achieved after 80 min of NO_2 inlet. NO did not return to a zero level and dwelt at 24 ppm even until 110 min, which was related to the equilibrium decomposition of NO_2 ($2NO_2 \leftrightarrow 2NO + O_2$) that may occur in gas-phase (see Fig. 1e).

The plateau of constant outlet NO (335 ppm) from 5 to 11 min and the absence of NO_2 in this period indicate that NO_2 is selectively adsorbed, and simultaneously releases NO. That

Table 2
Volumetric determination of NO_x desorption on the $Ag/Al_2O_3/Al$ catalyst at 298 K

Adsorption gas stream	TPD/TPSR gas stream	Desorption amount of NO_x (μmol g^{-1})			
		LT peak	HT peak	Overall peak	$\Delta NO_{x_{desorbed}}$ [a]
A: 1000 ppm NO/He	He	–	–	21.5	–
	5000 ppm C_3H_6/He	–	–	20.8	0.7
	5000 ppm C_3H_6/15% O_2/He	–	–	13.0	8.6
B: 1000 ppm NO/15% O_2/He (500 K)[b]	He	119.7	203.2	322.9	–
	5000 ppm C_3H_6/He	125.5	170.1	295.7	27.2
	5000 ppm C_3H_6/15% O_2/He	112.3	110.5	222.8	100.1
C: 1000 ppm NO_2/He (425 K)[b]	He	38.4	485.8	524.2	–
	5000 ppm C_3H_6/He	41.8	423.8	465.6	58.5
	5000 ppm C_3H_6/15% O_2/He	35.1	353.2	388.3	135.9

[a] $\Delta NO_{x_{desorbed}}$ = NO_x desorption in He–NO_x desorption in C_3H_6 (or $C_3H_6 + O_2$).
[b] Boundary temperature point between low temperature peak and high temperature peak in TPD/TPSR.

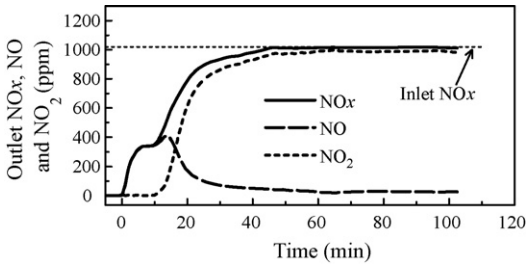

Fig. 7. Dependence of outlet NO_x, NO and NO_2 concentrations on adsorption time of the $Ag/Al_2O_3/Al$ catalyst in flowing 1000 ppm NO_2/He at 298 K.

is, there is a transformation of NO_2 into NO. Considering that in this period the 1015 ppm of NO_2 in the feed reacted entirely, the molar ratio of reacted NO_2 to NO formation is ca. 3.0.

Apostolescu et al. [41] reported a mechanism for the formation of surface nitrate species concluded from the adsorption/desorption phenomena of NO_2 on γ-alumina. They proposed that at first, the disproportionation of adsorbed NO_2 resulted in the formation of nitrosyl and nitrate (Eq. (1)). NO^+ rapidly undergoes reaction with the surface oxide to form nitrite (Eq. (2)). Nitrite then reacts with the strong oxidant NO_2, leading to the formation of NO_3^- as well as gaseous NO.

$$2NO_2(ads) \leftrightarrow NO^+(ads) + NO_3^-(ads) \quad (1)$$

$$NO^+(ads) + O^{2-}(s) \leftrightarrow NO_2^-(ads) \quad (2)$$

$$NO_2^-(ads) + NO_2(g) \leftrightarrow NO_3^-(ads) + NO(g) \quad (3)$$

$$3NO_2(g) + O^{2-}(s) \leftrightarrow 2NO_3^-(ads) + NO(g) \quad (4)$$

The overall reaction (Eq. (4)) indicates a stoichiometry of three NO_2(g) reacting per one NO(g) released. The stoichiometric ratio shows very good accordance with the experimental data of the plateau observed in Fig. 7. Furthermore, over the entire 80 min period in which NO_x adsorption occurred, volumetric determination of the outlet profiles of NO_2 and NO gives the reacted NO_2 as 798.3 μmol g^{-1} and the released NO_2 as 263.0 μmol g^{-1}, by subtracting the background found in a corresponding blank experiment. The molar ratio of the reacted

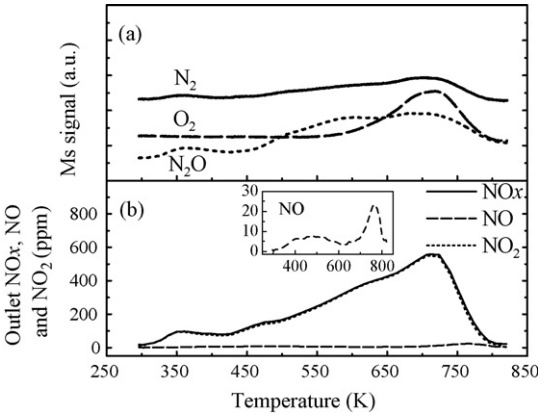

Fig. 8. TPD profiles (a) outlet ms-signals of N_2, O_2 and N_2O; (b) outlet concentrations of NO_x, NO and NO_2, in flowing He after exposure of the $Ag/Al_2O_3/Al$ catalyst to 1000 ppm NO_2/He.

NO_2 over the released NO is also around 3.0. Thus, the adsorption model proposed by Apostolescu et al. is considered also applicable to the case of NO_2 adsorption on the $Ag/Al_2O_3/Al$ catalyst. In addition, Pazé et al. [42] proposed a very similar mechanism for the NO_2 adsorption on a dehydroxylated alumina surface.

Fig. 8 shows the TPD profiles of the $Ag/Al_2O_3/Al$ catalyst after exposure to NO_2 in flowing He. Similar to Fig. 6, both NO_2 and NO desorption profiles displayed two significant peaks: a LT desorption peak (<425 K) and a HT desorption peak (>425 K), though the NO evolution was much weaker than that of NO_2. The desorption profile of NO_2 in the high temperature region gradually climbed with increasing temperature, passing through a weak shoulder peak at 612 K and having a maximum at 717 K, and was accompanied with the evolution of O_2, N_2, N_2O. Considering the interpretation of (NO/O_2)-TPD and NO_2-data reported by several groups [34,41–47], this HT desorption peak for NO_2 is assigned to the decomposition of surface nitrate species, because NO_2 and O_2 were simultaneously produced according to Eq. (5).

$$2NO_3^-(ads) \leftrightarrow 2NO_2(g) + 0.5O_2(g) + O^{2-}(s) \quad (5)$$

The shoulder peak for NO_2 at 612 K is explained in that there are three types of surface nitrates on Ag/alumina with thermal stability in the order monodentate > bidentate > bridbridging nitrates (NO_3^-) [46]. Although the LT desorption peak for NO_2 is generally ascribed to molecularly chemisorbed NO_2, Apostolescu et al. [41] and Burch et al. [47] proposed another possibility that the formation of NO_2 originated from the decomposition of nitrosyl cation, which could be referred to the reaction of NO^+ with NO_3^- to form NO_2 according to the back reaction of Eq. (1). They reported some of the nitrosyl species were still present on the catalyst surface even after saturation, whereby NO^+ was desorbed at 373 K, a similar temperature to our result. However, the existence of nitrosyl species after saturation and purgation, which can be easily removed by evacuation [48], is still disputed.

The very weak LT peak for NO is associated with the decomposition of nitrite that is still present in trace amounts, according to the back reaction of Eq. (2). For the formation of NO in the high temperature range, the thermal decomposition of the NO_2 desorbed due to thermodynamics is considered an interpretation.

Comparison of the HT peak in Fig. 6 with that in Fig. 8 showed great similarity, i.e., (1) both HT desorption peaks appeared in the same temperature range, accompanied by desorption peaks of O_2, N_2 and N_2O; (2) only a little NO was found in the high temperature region. Therefore, the HT desorption peak obtained after exposure to NO/O_2/He should also be assigned to the surface nitrate species. The stronger LT desorption peak for NO (peaking at 359 K) in Fig. 6 was associated with the desorption of much more nitrite species formed during the coadsorption of NO and O_2, because no oxygen evolution was found to accompany the NO desorbed.

NO chemisorption can be divided into reactive and non-reactive adsorption. During non-reactive adsorption, surface

mononitrosyl and dinitrosyl complexes are formed [36]. The gaseous oxygen adsorbs and dissociates into surface oxygen O^{2-}(s), and reacts with the nitrosyl components to form nitrite species according to Eq. (2). The formation of nitrate species in the NO/O_2/He gas stream is considered to probably proceed according to Eqs. (1)–(3). That is, NO_2, which originates from the oxidation of NO with O_2, directly participates in the adsorption process. In addition, the time-dependent phenomenon of the formation of nitrite species during NO_x adsorption revealed by DRIFT, reported by other groups [34,41], provides another possibility that in the presence of oxygen, NO firstly adsorbs into nitrite, and then this nitrite is oxidized into nitrate with gaseous NO_2 via Eq. (3).

A reference TPD test after exposure of the catalyst to 1000 ppm NO_2/15% O_2/He was conducted in flowing He (not shown here) to further study the effect of oxygen. In comparison with Fig. 8, this TPD result does not show any noticeable difference in the shape, temperature and area of the desorption peak. Both NO_x adsorption profiles are also analogous for main adsorption characteristics such as the absence of NO_2 in the start period, the plateau of NO released, and the adsorption amount of NO_x. The result demonstrates that the effect of oxygen on the formation of nitrate species in the coadsorption of NO and O_2 is to oxidize NO into NO_2, and then the gaseous NO_2 will directly adsorb into nitrate (or oxidize nitrites into nitrates). In addition, the NO_x adsorption capacity in Fig. 7 was ca. 534.6 μmol g^{-1}, which was significantly more than that in NO/O_2/He. The relatively small amount of gaseous NO_2 formation is considered responsible for the smaller NO_x adsorption capacity and the formation of more nitrite species.

In the absence of oxygen, as described in Fig. 4, the NO uptake was very poor, and there was only a weak LT desorption peak for NO, which should be attributed to the molecularly chemisorbed NO or the decomposition of nitrite species because it was not accompanied with the simultaneous evolution of NO_2 or O_2. Nevertheless, a signal of N_2O as well as N_2 with very small intensity was recorded at high temperatures. In comparison with Fig. 6 or Fig. 8 in which the nitrate species were present, the decomposition of a minute amount of nitrate is a seemingly reasonable interpretation for this formation of N_2O and N_2. The necessary oxygen to form nitrate is suggested to come from the dissociation of NO on silver surfaces [34]. The desorption of oxygen was not detected under this condition, probably because the trace amount of oxygen was strongly bounded on silver surfaces and might be slowly released at high temperatures [44]. Another possibility refers to the nitrosyl complexes, a plausible intermediate to produce N_2O and N_2, which was evidenced by N_2O formation accompanying the decrease in IR bands for nitrosyl species [44,49].

It should be noted that the influence of water on the NO_x adsorption has not been investigated in this paper. However, it is a fact that in the presence of water the NO_2 adsorption chemistry on Ag/Al_2O_3 is entirely different. Brosius et al. [50] reported that at 423 K Ag/Al_2O_3 did not adsorb any NO in the presence of 12% water in a gas mixture of 500 ppm NO_2/500 ppm NO/6% O_2/12% H_2O/He. They stated that the nitrate formation proceeded through the formation of nitric acid from NO_2 and water. The interaction of NO_2 is confined to the framework of oxygen whereas in the presence of water, NO_2 also interacts with surface hydroxyl groups.

3.3. TPSR studies

In previous work, the reactivity of surface NO_x species formed after adsorption of NO/O_2 with various hydrocarbons or oxygenates, such as propene/propane [2,4,25,46], higher hydrocarbons (C4–C8) [8,25], and ethanol/methanol [46], has been examined over alumina [4] and silver/alumina catalysts [2,4,8,25,46] by FTIR or TPR measurements. Consistently, different research groups have reported high reactivity of adsorbed NO_x species to these reductants, confirming the importance of these species as intermediates for the SCR of NO. According to the aforementioned experimental results, on the anodic alumina supported silver catalyst after exposure to different adsorption gases, the formation of surface nitrite/nitrate species was identified by adsorption and TPD tests. However, to our knowledge, no sufficient information is available for the reactivity of adsorbed NO_x species with C_3H_6 over the anodic alumina supported silver catalyst, especially for the reactivity difference of the adsorbed NO_x species formed through different adsorption processes (NO/He, NO/O_2/He and NO_2/He) in different reaction systems (C_3H_6/He and C_3H_6/O_2/He). Consequently, in this work, TPSR tests were performed by flowing C_3H_6/He or C_3H_6/O_2/He on Ag/Al_2O_3/Al after exposure to different adsorption gas streams.

Fig. 9 shows TPSR profiles in a 5000 ppm C_3H_6/15% O_2/He gas stream after ''NO only'' adsorption. The desorption profile of NO was similar to that in the He stream, except for a slight decrease. Apparent and continuous propene consumption initiated at ca. 550 K and increased gradually with increasing temperature, and was accompanied with a remarkable formation peak for CO (Fig. 9b). The fact that the profiles of m/z = 28 and 44 are approximately mirror image responses to the consumption profile of C_3H_6, indicates the TPSR profiles should be mainly associated with the oxidation reaction of propene with oxygen, due to the poor adsorption of NO.

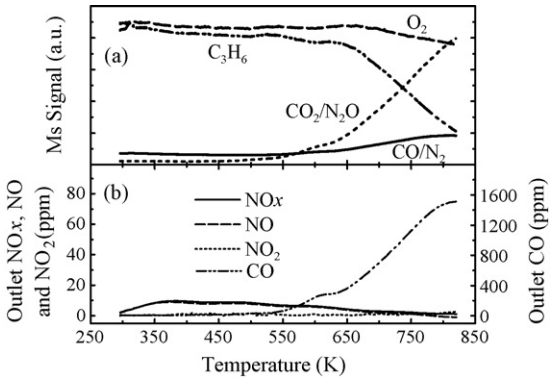

Fig. 9. TPSR profiles (a) outlet ms-signals of CO/N_2, O_2, C_3H_6 and CO_2/N_2O; (b) outlet concentrations of NO_x, NO, NO_2 and CO, in flowing 5000 ppm C_3H_6/15% O_2/He after exposure of the Ag/Al_2O_3/Al catalyst to 1000 ppm NO/He.

However, several barely detectable shoulder peaks in the profiles of $m/z = 28$ (Fig. 9a), $m/z = 44$ (Fig. 9a), propene (Fig. 9a) and CO (Fig. 9b) were recorded near 623 K. The reaction between propene, oxygen and the trace amount of adsorbed NO_x species is considered to lead to these shoulder peaks. In Table 2, when changing the gas stream from He to C_3H_6/O_2/He, the difference in the desorption amount of NO_x, $\Delta NO_{x_{desorbed}} = 8.6\ \mu mol\ g^{-1}$, demonstrated that some adsorbed NO_x species reacted with propene to form N_2 and N_2O. Thus, for the formation profile of $m/z = 28$, the formation of nitrogen could not be excluded, especially near 623 K. That is, the $m/z = 28$ ms-signal was in fact from both the reduction product (N_2, $m/e = 28$) of NO and the oxidation product (CO, $m/z = 28$) of propene. Similarly, the formation profile with $m/z = 44$ was from CO_2 ($m/z = 44$) and N_2O ($m/z = 44$).

To examine the reactivity of adsorbed NO_x species, a TPSR test of $Ag/Al_2O_3/Al$ after the coadsorption of NO and O_2 was conducted in the same gas stream of 5000 ppm C_3H_6/15% O_2/He, and the result is shown in Fig. 10. All NO_x desorption profiles (NO_x, NO, and NO_2) displayed a LT desorption peak (<500 K) and a HT desorption peak (>500 K), as shown in Fig. 6. The LT peak for NO_x was nearly the same as that in the TPD test, considering shape, peak maximum temperature, and area (as shown in Table 2). The result that no new product was detected shows no reaction took place between the surface nitrite species and propene. When the temperature exceeded 500 K, however, an obviously different desorption behavior was exhibited. From 500 to 573 K, the nitrate species mainly decomposed into NO_2, similar to what is seen in Fig. 6 but at a more rapid decomposition rate. As the temperature further increased (>573 K), the NO evolution increased considerably, whereas it maintained a relatively low level in Fig. 6. The desorption peak for NO_x at 616 K gradually disappeared in the C_3H_6/O_2/He gas stream when the temperature exceeded 660 K. Conversely, the apparent propene consumption initiated at 573 K, which coincided with the "light-off" temperature in the steady-state reaction, and then passed through a remarkable shoulder peak at 623 K. Above 660 K, the consumption of propene increased in complete analogy to results shown in Fig. 9. Simultaneously, the formation of CO (Fig. 10b) and CO_2 (overlapped with the formation of N_2O in Fig. 10a) as well as the consumption of oxygen started at 573 K. Shoulders appeared at the same temperature of 623 K. The formation of CO (in Fig. 10b) was observed to be an exact mirror image of the consumption of propene. Though the ms-signal of CO_2 overlapping with N_2O, the formation profile of $m/z = 44$ shows good coincidence with the consumption of propene, maybe due to low production of N_2O. These results indicate that propene was oxidized to CO and CO_2.

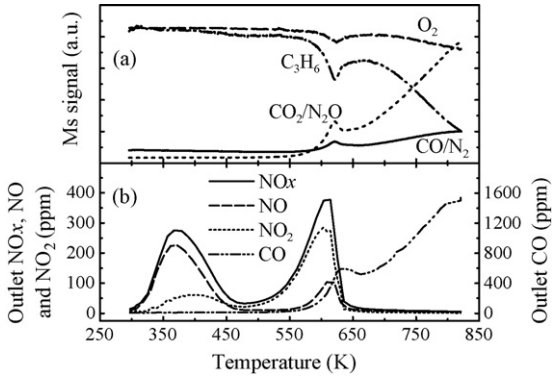

Fig. 10. TPSR profiles (a) outlet ms-signals of CO/N_2, O_2, C_3H_6 and CO_2/N_2O; (b) outlet concentrations of NO_x, NO, NO_2 and CO, in flowing 5000 ppm C_3H_6/15% O_2/He after exposure of the $Ag/Al_2O_3/Al$ catalyst to 1000 ppm NO/15% O_2/He.

The appearance of the obvious shoulder peak from 573 to 660 K is the most obvious difference between Figs. 9 and 10. In this region, the consumption of C_3H_6 exhibited some coincidence with the decomposition of nitrate in that the shoulder peak for C_3H_6 initiated at 573 K and was accompanied by the apparent difference in NO/NO_2 desorption (cf. Figs. 6 and 10). More NO was desorbed, and it disappeared after the complete desorption of nitrate. This coincidence indicates that the reaction between surface nitrate species and propene started with propene oxidation from 573 K, and ended with the complete consumption of nitrate at 660 K. Unfortunately, in Fig. 10, identification of the formation of N_2 and N_2O was difficult, because their ms-signals overlapped with the formation ms-signals of CO and CO_2 from propene oxidation, respectively. Nevertheless, the decreased amount of desorbed NO_x, $\Delta NO_{x_{desorbed}} = 100.1\ \mu mol\ g^{-1}$, confirmed to some extent that 50% of nitrate species (HT peak) was reduced by propene into N_2 and N_2O, which is also believed to occur in the shoulder peak region because no noticeable formation signal was observed in other temperature regions.

The increased desorption amount of NO in the shoulder peak region is attributed to the incomplete reduction of NO_2 produced from the decomposition of nitrate with propene, as discussed in Figs. 1e and 2. The more rapid desorption rate of NO_2 at the front of the shoulder peak region is considered responsible for the slight increase in NO_2 yield in the case of $NO/C_3H_6/O_2$/He, as shown in Fig. 1d.

When introducing oxygen into the gas streams, propene will react not only with nitrate species but also with oxygen. These two parallel reactions compete with each other, and show strong dependence on reaction temperature as well as reaction conditions. As shown in Fig. 10, the consumption profiles of propene and oxygen as well as the formation profiles of CO and CO_2 can be divided into two regions across 660 K. In the first region, propene consumption was accompanied by the desorption of nitrate species and the formation of N_2 and N_2O, and gave a shoulder peak at 623 K. In the second region, due to the complete decomposition of nitrate species, propene only combusted directly with oxygen. The valley in the profile of propene consumption at 623 K reflects the different rates of the propene selective reduction of NO_x and propene direct combustion with oxygen. When NO_x and O_2 coexist in the feed, propene will preferentially and selectively reduce surface nitrate species into N_2 and N_2O, rather than react directly with oxygen to form CO_x. The priority of the reaction of propene with surface nitrates to form oxygen clearly demonstrates the selective reduction of NO_x by propene over silver catalysts is due to the formation of the more reactive nitrate species.

Fig. 1b described the result that when using NO_2 instead of NO in the case of 1000 ppm NO or NO_2/1000 ppm C_3H_6/2% O_2/He, propene oxidation was remarkably improved, whereas the ratio of increased oxygen atoms from NO_2 to total oxygen atoms was just 4.8%. A similar result was observed when examining the influence of NO on propene oxidation. As shown in Fig. 11, under excess oxygen conditions (15%), introducing a small amount of NO (1000 ppm) greatly affects propene oxidation, though the increased oxygen atoms were almost negligible (0.6%). The effect of NO could be divided into two regions below and above the "light-off" temperature at 573 K. In the region above 573 K, the presence of NO substantially improved propene oxidation. On the contrary, in the region below 573 K, it inhibited propene oxidation and acted as a catalyst poison. Referring to the discussion above, the promotional effect of NO is associated with the higher reaction rate of the reaction of propene with nitrate species rather than the direct oxidation with oxygen. In the low temperature region, the surface nitrate species occupy active sites, and the decomposition does not yet happen, which inhibits the propene oxidation. Similarly, the much stronger NO_x adsorption capacity of NO_2, compared with that of NO, is one possible interpretation for the promoted propene conversion by replacing NO by NO_2 in the case of NO or NO_2/1000 ppm C_3H_6/2% O_2/He.

In the discussion above, the effect of oxygen on the present reaction was mainly described as a promoter of NO_x adsorption and a competitive oxidant with nitrate species. This conclusion is seemingly reasonable because it can explain experimental phenomena in Fig. 1 such as the enhanced NO_x conversion when switching from NO to NO_2 in the "propene only" case (without oxygen), the enhanced NO_x conversion with increasing oxygen in the NO/C_3H_6/O_2/He case, and the decrease in NO_x conversion after propene conversion reaching 100% at high temperatures. However, the enhanced NO_x conversion when introducing oxygen into NO_2/C_3H_6/He is hard to explain, because no noticeable increase in the NO_2 adsorption capacity was observed when introducing oxygen into the NO_2 gas stream (see Table 1). To comprehensively study the effect of oxygen on the present reaction, a TPSR test was conducted in a C_3H_6/He gas stream (without O_2) after the coadsorption of NO and O_2, as shown in Fig. 12. Below a temperature of 623 K in which the desorption peak of nitrate species appeared, the desorption behavior of nitrate was very similar to that in Fig. 10, except for more NO evolution from 500 to 623 K. With the temperature further increasing, desorbed NO_x gradually disappeared in the propene gas stream before 723 K, indicating the desorption and/or consumption of nitrate proceeded at a lower rate than that in Fig. 10. No remarkable consumption peak was observed in the ms-signal of propene, except for a slight decrease in intensity at 673 K. According to Table 2, it is obvious that the absence of oxygen decreased the reacted amount of desorbed NO_x ($\Delta NO_{x_{desorbed}}$) from 100.1 to 27.2 μmol g^{-1}. These results suggest that in the presence of oxygen, the surface nitrate species might react with a more active reductant intermediate to form nitrogen, rather than directly reacting with propene. The partially oxygenated (activated) propene with oxygen is believed to be a main origin of the active reductant intermediate. Though a direct oxygen source was not provided in the gas stream in Fig. 10, the decomposition of nitrate species could supply a little oxygen and NO_2 to activate propene, which is related to the smaller $\Delta NO_{x_{desorbed}}$ and the evolution of much more NO.

TPSR measurements conducted in C_3H_6/He and in C_3H_6/O_2/He gas stream, after exposure of the Ag/Al_2O_3/Al catalyst to NO_2/He, are depicted in Figs. 13 and 14, respectively. Comparisons with Figs. 10 and 12 do not show any remarkable difference in reactivity characteristics. In Fig. 14, the shoulder peaks of propene consumption, oxygen consumption, CO formation and CO_2/N_2O formation were observed at the temperature of 623 K, as for Fig. 10. Introducing oxygen into the C_3H_6 gas stream considerably promoted the reduction of nitrate, and the amount of reacted nitrate increased from 58.5 to 135.8 μmol g^{-1}. These similar results illuminate that there was no difference in the reactivity with propene between the nitrate from the coadsorption of NO and O_2 and that from the NO_2 adsorption.

In the following, the knowledge obtained through adsorption, TPD and TPSR will be used to explain the results of the

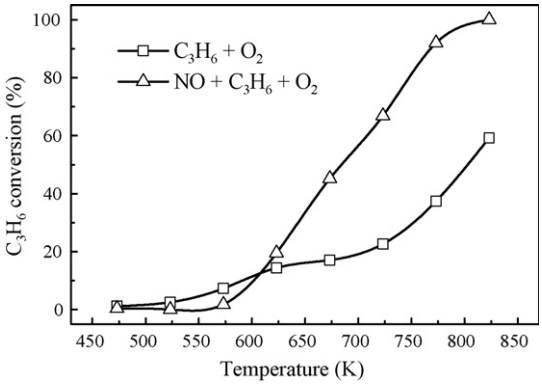

Fig. 11. C_3H_6 conversion of Ag/Al_2O_3/Al in the absence and presence of NO as a function of temperature. (NO 0 or 1000 ppm, O_2 15.0%, C_3H_6 5000 ppm) *Reactor i.d.: 15 mm. Loading density: 2.0 $cm^2_{catalyst}(g_{quartzsand})^{-1}$.

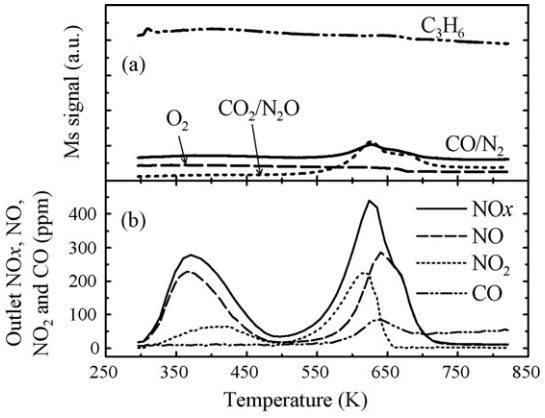

Fig. 12. TPSR profiles (a) outlet ms-signals of CO/N_2, O_2, C_3H_6 and CO_2/N_2O; (b) outlet concentrations of NO_x, NO, NO_2 and CO, in flowing 5000 ppm C_3H_6/He after exposure of the Ag/Al_2O_3/Al catalyst to 1000 ppm NO/15% O_2/He.

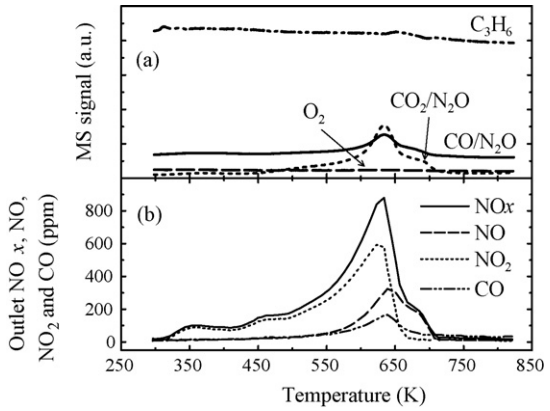

Fig. 13. TPSR profiles (a) outlet ms-signals of CO/N_2, O_2, C_3H_6 and CO_2/N_2O; (b) outlet concentrations of NO_x, NO, NO_2 and CO, in flowing 5000 ppm C_3H_6/He after exposure of the $Ag/Al_2O_3/Al$ catalyst to 1000 ppm NO_2/He.

steady-state test shown in Fig. 1. In the absence of oxygen, the NO adsorption capacity is very poor (see Figs. 3 and 4), and gas-phase NO hardly directly reacts with propene, which leads to the non-activity of propene in reducing NO. Increasing the oxygen concentration accelerates the formation of the surface nitrate species and the activated propene, and thus NO reduction is ultimately and substantially promoted. Meanwhile, the ''nitrate poisoning'' delays the ''light-off'' temperature of propene oxidation from 473 to 573 K (see Fig. 9). In the absence of oxygen (or in the presence of 2% low concentration oxygen), when introducing NO_2 to replace NO, the increased NO_x adsorption capacity causes an improved NO_x reduction. In addition, the stronger oxidation ability of NO_2, compared with that of NO, is also non-negligible especially in the absence of oxygen, due to its effect on activating propene. In the case of NO_2/C_3H_6/He, the decreased NO_x conversion above 673 K is attributed to the incomplete reduction of NO_2 with propene into NO (see Figs. 1e and 2). With increasing oxygen concentration, the difference in the NO_x adsorption capacity between NO and NO_2 decreases, and the superiority of NO_2 over NO in activating propene also gradually disappears due to the presence of excess oxygen. Eventually, the difference in the NO_x conversion between NO and NO_2 gradually decreases. In addition, the incomplete reduction of NO_2 with reductants into

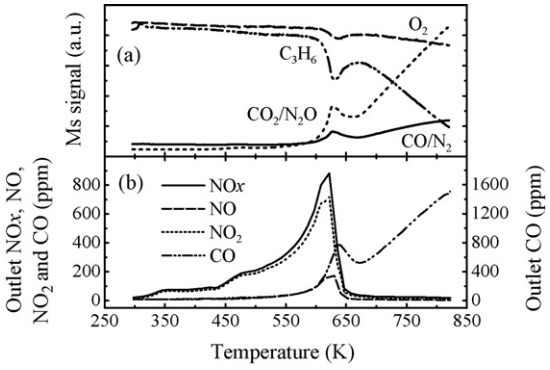

Fig. 14. TPSR profiles (a) outlet ms-signals of CO/N_2, O_2, C_3H_6 and CO_2/N_2O; (b) outlet concentrations of NO_x, NO, NO_2 and CO, in flowing 5000 ppm C_3H_6/15% O_2/He after exposure of the $Ag/Al_2O_3/Al$ catalyst to 1000 ppm NO_2/He.

NO might also be aggravated with the appearance of more partially oxygenated propene, which can occur even in gas-phase. However, the disappearance of the reactivity difference between NO and NO_2 in the presence of 15% oxygen (see Fig. 1a), which seems contradictory to the fact that the NO_x adsorption capacity in NO_2 is still far higher than that in NO/O_2/He even if 15% O_2 is present (Table 2, NO/O_2: 322.9 μmol g^{-1}; NO_2: 514.2 μmol g^{-1}), requires new explanation. The slower activation rate of propene is considered a possibility, i.e., it may be a controlling step of the kinetics of the overall reaction. In Table 2, $\Delta NO_{x_{desorbed}}$ in the C_3H_6/O_2/He gas stream slightly increased by 35.7 μmol g^{-1} (from 100.1 to 135.8 μmol g^{-1}), whereas the overall NO_x adsorption capacity substantially improved by 191.3 μmol g^{-1} (from 322.9 to 514.2 μmol g^{-1}), when using the catalyst exposed to NO_2 to replace that exposed to NO/O_2. The relatively slow activation rate of propene is associated with the poor oxidation ability of silver (compared with Pt, Cu, and so on) and ''nitrate poisoning''. A further study is now in progress to find direct evidence.

In this paper, the de-NO_x activity of a metal monolithic plate-type anodic alumina supported Ag catalyst was investigated under oxygen-rich conditions. The favorable de-NO_x activity shows that the application of the anodic alumina catalyst in controlling NO_x exhaust is a promising area, especially for the NO_x exhaust from diesel vehicles in which a more compact reactor, smaller pressure drop and more favorable thermal conductivity are required. Though the mechanism of HC-SCR was also studied over this catalyst by NO_x adsorption and TPD and TPSR measurements, the discussion is insufficient because the influences of the Ag state (Ag(0) and Ag(I)) and the presence of water have not been considered. They are very important in the de-NO_x activity of the catalyst. Especially, it is possible that the state of Ag will be modified under different reaction conditions. Even so, it was reported that even trace amounts of reducing agents such as 500 ppm propene in the presence of 2.5% O_2 caused the reduction of some silver [20]. Further study of these influences over our catalyst is now in progress and will be discussed elsewhere later.

4. Conclusions

In the absence of oxygen, no remarkable uptake of NO was detected at ambient temperature. In contrast, a considerable amount of surface ads-NO_x species was formed on the $Ag/Al_2O_3/Al$ catalyst after exposure to NO_2, accompanied with the formation of NO. The quantitative analysis showed that the mole ratio of reacted NO_2 to released NO was 3.0. After the coadsorption of NO and O_2, the formation of nitrate species was also confirmed, but as a smaller amount than that in NO_2 adsorption. The direct participation of NO_2 in the adsorption process and the oxidation of nitrite species with NO_2 were believed to be main reasons for the formation of nitrate species in NO/O_2 coadsorption. The effect of oxygen on the formation of nitrate species was associated with the oxidation of NO into NO_2.

The result of TPSR in C_3H_6/O_2/He demonstrated the surface nitrate species (but not nitrite species) could be effectively and preferentially reduced by propene. When introducing oxygen into the propene gas stream of the TPSR test, the significantly increased amount of reacted nitrate species undoubtedly showed the promotional effect of oxygen on activating propene. The pathway for the selective reduction of NO_x in the presence of excess oxygen was proposed to pass through the selective reduction of adsorbed nitrate species with the activated propene. In addition, the surface nitrate species was found to be a catalyst poison at low temperatures due to its inhibitory effect on activating propene, but was a promoter of de-NO_x activity at high temperatures (>573 K).

The enhanced NO_x conversion when replacing NO by NO_2 was attributed to the stronger NO_x adsorption capacity and oxidation ability of NO_2, compared with that of NO. With increasing oxygen concentration, the difference gradually decreases, and finally disappears in a high excess of oxygen. Besides the decreased difference in NO_x adsorption capacity and the incomplete gaseous reduction of NO_2 into NO with reductant agent, the slower activation rate of propene was considered a supplementary interpretation for this disappearance.

References

[1] A. Keshavaraja1, X. She, M. Flytzani-Stephanopoulos, Appl. Catal. B: Environ. 27 (2000) L1.
[2] A. Martínez-Arias, M. Fernández-García, A. Iglesias-Juez, J.A. Anderson, J.C. Conesa, J. Soria, Appl. Catal. B: Environ. 28 (2000) 29.
[3] H.W. Jen, Catal. Today 42 (1998) 37.
[4] F.C. Meunier, J.P. Breen, V. Zuzaniuk, M. Olsson, J.R.H. Ross, J. Catal. 187 (1999) 493.
[5] F.C. Meunier, R. Ukropec, C. Stapleton, J.R.H. Ross, Appl. Catal. B: Environ. 30 (2001) 163.
[6] T.N. Angelidis, N. Kruse, Appl. Catal. B: Environ. 34 (2001) 201.
[7] S. Satokawa, K. Yamaseki, H. Uchida, Appl. Catal. B: Environ. 34 (2001) 299.
[8] K. Shimizu, J. Shibata, H. Yoshida, A. Satsuma, T. Hattori, Appl. Catal. B: Environ. 30 (2001) 151.
[9] K. Shimizu, A. Satsuma, T. Hattori, Appl. Catal. B: Environ. 25 (2000) 239.
[10] N. Bion, J. Saussey, M. Haneda, M. Daturi, J. Catal. 217 (2003) 47.
[11] T. Miyadera, Appl. Catal. B: Environ. 2 (1993) 199.
[12] K. Masuda, K. Tsujimura, K. Shinado, T. Kato, Appl. Catal. B: Environ. 8 (1996) 33.
[13] T.E. Hoost, R.J. Kudla, K.M. Kollins, M.S. Chattha, Appl. Catal. B: Environ. 13 (1997) 59.
[14] Z. Li, M. Flytzani-Stephanopoulos, J. Catal. 182 (1999) 313.
[15] K.A. Bethke, H.H. Kung, J. Catal. 172 (1997) 93.
[16] R. Burch, J.P. Breen, F.C. Meunier, Appl. Catal. B: Environ. 39 (2002) 283.
[17] M.C. Kung, K.A. Bethke, J. Yan, J.-H. Lee, H.H. Kung, Appl. Surf. Sci. 121–122 (1997) 261.
[18] T. Miyadera, Appl. Catal. B: Environ. 13 (1997) 157.
[19] A. Satsuma, J. Shibata, A. Wada, Y. Shinozaki, T. Hattori, Stud. Surf. Sci. Catal. 145 (2003) 235.
[20] N. Bogdanchikova, F.C. Meunier, M. Avalos-Borja, J.P. Breen, A. Pestryakov, Appl. Catal. B: Environ. 36 (2002) 287.
[21] T. Furusawa, L. Lefferts, K. Seshan, K. Aika, Appl. Catal. B: Environ. 42 (2003) 25.
[22] H. He, J. Wang, Q. Feng, Y. Yu, K. Yoshida, Appl. Catal. B: Environ. 46 (2003) 365.
[23] K. Sato, T. Yoshinari, Y. Kintaichi, M. Haneda, H. Hamada, Appl. Catal. B: Environ. 44 (2003) 67.
[24] S. Satokawa, J. Shibata, K. Shimizu, A. Satsuma, T. Hattori, Appl. Catal. B: Environ. 42 (2003) 179.
[25] K. Shimizu, J. Shibata, A. Satsuma, T. Hattori, Phys. Chem. Chem. Phys. 3 (2001) 880.
[26] R. Burch, J.P. Breen, C.J. Hill, B. Krutzsch, B. Konrad, E. Jobson, L. Cider, K. Eränen, F. Klingstedt, L.-E. Lindfors, Top. Catal. 30 (2004) 19.
[27] H. Kameyama, K. Murata, S. Terai, Y. Toyoshima, J. Surf. Finish. Soc. Jpn. 46 (1995) 425.
[28] H. Kameyama, J. Toyoshima, Japanese Patent Disclosure H08-243408 (1996).
[29] Y. Guo, M. Sakurai, H. Kameyama, A. Matsuyama, Y. Kudoh, J. Chem. Eng. Jpn. 36 (2003) 1471.
[30] Q. Zhang, A. Iqbal, M. Sakurai, T. Kitajima, H. Takahashi, M. Nakaya, T. Ootani, H. Kameyama, Seventh World Congress of Chemical Engineering, Glasgow, Scotland, (2005), pp. 16–27.
[31] J.M. García-Cortés, J. Pérez-Ramírez, M.J. Illán-Gómez, F. Kapteijn, J.A. Moulijn, C. Salinas-Martínez de Lecea, Appl. Catal. B: Environ. 30 (2001) 399.
[32] H. Hamada, Catal. Today 22 (1994) 21.
[33] X. Bao, U. Wild, M. Muhler, B. Pettinger, R. Schlögl, G. Ertl, Surf. Sci. 425 (1999) 224.
[34] J. Müslehiddinoğlu, M. Albert Vannice, J. Catal. 217 (2003) 442.
[35] D.Y. Zemlyanov, A. Nagy, R. Schlögl, Appl. Surf. Sci. 133 (1998) 171.
[36] D.Y. Zemlyanov, G. Weinberg, U. Wild, R. Schlögl, Catal. Lett. 64 (2000) 113.
[37] D. Zemlyanov, R. Schlögl, Surf. Sci. 470 (2000) L20.
[38] K.U. Von Raben, P.B. Dorain, T.T. Chen, R.K. Chang, Chem. Phys. Lett. 95 (1983) 269.
[39] D.A. Outka, R.J. Madix, G.B. Fisher, C. Dimaggio, Surf. Sci. 179 (1987) 1.
[40] F. Bartollucci, A. Otto, Surf. Rev. Lett. 1 (1994) 561.
[41] N. Apostolescu, T. Schröder, S. Kureti, Appl. Catal. B: Environ. 51 (2004) 43.
[42] C. Pazé, G. Gubitosa, S. Orso Giacone, G. Spoto, F.X. Llabrés i Xamena, A. Zecchina, Top. Catal. 30 (2004) 169.
[43] C. Shi, M.J. Cheng, Z.P. Qu, X.H. Bao, Appl. Catal. B: Environ. 51 (2004) 171.
[44] C. Shi, M.J. Cheng, Z.P. Qu, X.F. Yang, X.H. Bao, Appl. Catal. B: Environ. 36 (2002) 173.
[45] X. She, M. Flytzani-Stephanopoulos, J. Catal. 237 (2006) 79.
[46] S. Kameoka, Y. Ukisu, T. Miyadera, Phys. Chem. Chem. Phys. 2 (2000) 367.
[47] R. Burch, J.A. Sullivan, T.C. Watling, Catal. Today 42 (1998) 13.
[48] V.A. Sadykov, S.L. Baron, V.A. Matyshak, G.M. Alikina, R.V. Bunina, A.Y. Rozovskii, V.V. Lunin, E.V. Lunina, A.N. Kharlanov, A.S. Ivanova, S.A. Veniaminov, Catal. Lett. 37 (1996) 157.
[49] M. Iwamoto, H. Yahiro, N. Mizuno, W.X. Zhang, Y. Mine, S. Futukawa, J. Phys. Chem. 96 (1992) 9360.
[50] R. Brosius, K. Arve, M.H. Groothaert, J.A. Martens, J. Catal. 231 (2005) 344.